Check for updates

AGU ADVANCING EARTH AND SPACE SCIENCE

Space Weather

RESEARCH ARTICLE
10.1029/2022SW003129

Ionospheric Turbulence: A Challenge for GPS Loss of Lock Understanding

P. De Michelis[1], G. Consolini[2], A. Pignalberi[1], G. Lovati[1,3], M. Pezzopane[1], R. Tozzi[1], F. Giannattasio[1], I. Coco[1], and M. F. Marcucci[2]

[1]Istituto Nazionale di Geofisica e Vulcanologia, Rome, Italy, [2]INAF-Istituto di Astrofisica e Planetologia Spaziali, Rome, Italy, [3]Dipartimento di Fisica, Universitá di Roma Sapienza, Rome, Italy

Key Points:

- Global Positioning System (GPS) loss of lock events are discussed according to the dynamical status of the ionosphere
- Ionospheric irregularities at the base of the GPS loss of lock events present an intermittent turbulent nature
- Extremely high values of Rate Of change of electron Density Index are associated with GPS loss of lock events

Supporting Information:

Supporting Information may be found in the online version of this article.

Correspondence to:

P. De Michelis,
paola.demichelis@ingv.it

Citation:

De Michelis, P., Consolini, G., Pignalberi, A., Lovati, G., Pezzopane, M., Tozzi, R., et al. (2022). Ionospheric turbulence: A challenge for GPS loss of lock understanding. *Space Weather*, *20*, e2022SW003129. https://doi.org/10.1029/2022SW003129

Received 19 APR 2022
Accepted 15 JUN 2022

Author Contributions:

Conceptualization: P. De Michelis, G. Consolini
Data curation: A. Pignalberi, M. Pezzopane, R. Tozzi, F. Giannattasio, I. Coco
Formal analysis: P. De Michelis, G. Consolini, G. Lovati
Funding acquisition: P. De Michelis
Investigation: P. De Michelis, F. Giannattasio
Methodology: P. De Michelis, G. Consolini, A. Pignalberi, M. Pezzopane
Software: A. Pignalberi, M. Pezzopane
Writing – original draft: P. De Michelis
Writing – review & editing: G. Consolini, A. Pignalberi, G. Lovati, M. Pezzopane, R. Tozzi, F. Giannattasio, I. Coco, M. F. Marcucci

© 2022. The Authors.
This is an open access article under the terms of the Creative Commons Attribution License, which permits use, distribution and reproduction in any medium, provided the original work is properly cited.

Abstract Ionospheric irregularities may affect electromagnetic signals propagating through the ionosphere and consequently contribute to the malfunctioning of the Global Navigation Satellite Systems hindering their accuracy and reliability. In this study, we use data recorded on board two of the three satellites of the Swarm constellation (namely, Swarm A and Swarm B) from 15 July 2014 to 31 December 2021 to assess the possible dependence of the Global Positioning System (GPS) signals loss of lock on the presence of a specific kind of ionospheric irregularities. To accomplish this task we study the scaling features of the electron density fluctuations through the structure function analysis simultaneously to the occurrence of loss of lock events through measurements recorded by the Langmuir probes and the precise orbit determination antennas on board Swarm A and Swarm B satellites. We find that the plasma density irregularities in a turbulent state characterized by intermittent structures and extremely high values of the Rate Of change of electron Density Index can lead to GPS loss of lock events. This is always true at mid and high latitudes, especially inside the auroral oval. In the equatorial belt, this happens in at least 75% of identified GPS loss of lock events that basically coincide with the occurrence of plasma bubbles.

Plain Language Summary One of the natural factors that most contributes to the malfunctioning of Global Navigation Satellite Systems and leads to a degradation of their performance, accuracy and reliability, is represented by ionospheric irregularities. In this work, using data recorded by the European Space Agency Swarm constellation mission, we show for the first time that turbulence and extremely high values of the Rate Of change of electron Density Index are at the base of those ionospheric irregularities responsible for Global Positioning System loss of lock events. This result represents an important step forward in the perspective of developing a prediction model of such events, which could be significant in the framework of Space Weather purposes.

1. Introduction

Our society is becoming increasingly dependent on Global Navigation Satellite Systems (GNSS), such as the American Global Positioning System (GPS), the Russian GLONASS, the Chinese BeiDou, and the European GALILEO. These systems are fundamental for providing precise positioning on our planet, as well as for the timing and synchronization operations at the base of a vast number of activities. For this reason, critical infrastructures, such as power systems, railway control, maritime transport, civil and military aviation, communication technologies, government services, banking and finance systems, depend on the proper functioning of these navigation satellite systems (Moldwin, 2008). The crucial importance of a well-performing GNSS is further appreciated when realizing the degree of complexity of the interdependence between strategic infrastructures in our modern society.

One of the natural factors that contribute most to the degradation of GNSS signals, hindering the accuracy and reliability of these systems, is represented by ionospheric irregularities, that affect electromagnetic signals propagating through the ionosphere (Kintner & Seyler, 1985; Prikryl et al., 2011; Tsunoda et al., 1985). The ionospheric irregularities are plasma density variations that occur on scale sizes ranging between a few meters and hundreds of kilometers. Although they show a spatial and temporal distribution that are strongly controlled by geophysical parameters such as season, local time, longitude and latitude, they are often linked to disturbances of solar origin such as solar flares and coronal mass ejections (Kil et al., 2009; Tsunoda et al., 1985). This means that, especially in the case of significant solar events, such ionospheric structures may lead to one of the typical

effects of adverse space weather, that is, the degradation, at best, and the interruption, at worst, of the signals propagating toward a GNSS receiver. In the latter case, we observe a loss of lock (LoL) that is a condition for which a GNSS receiver can no longer track the signal sent by the satellite.

Some ionospheric plasma density irregularities are due to the occurrence of plasma turbulent processes. Turbulence is a phenomenon that each of us can observe directly. The arabesques formed by the smoke of a cigarette or the coffee poured into a glass of milk, the swirling motion of a stream or the motion of the meteorological perturbations observed by satellites are only a few of the examples where fluid turbulence is observed (Frisch, 1995; Tsinober, 2009). More generally, we can say that the term turbulence means the irregular and random motion of a fluid or a plasma. This definition, far from being exhaustive, tries to synthetically express one of the most complex and interesting phenomena in physics, that is at the base of a variety of mechanisms in which the redistribution of the system energy gives rise to important phenomena profoundly affecting the system itself. This happens in many natural systems and can be considered a crucial element also in the Earth's ionosphere where different driving mechanisms can trigger a turbulent state (Kelley, 2009). Numerical simulations and in situ observations have found that conditions boosting the development of turbulence may be built up in different regions of the ionosphere (Hysell & Shume, 2002; Kintner & Seyler, 1985). Indeed, it has been found that the F layer at both high and low latitudes can be characterized by irregularities, instabilities and turbulence covering a broad range of scales. Power spectra are often used to investigate and describe the occurrence of possible cascade processes of plasma density irregularities occurring in a turbulent state from large to small scales. In these conditions, power spectra are well described by power laws that extend over a wide range of scales and their slopes can be evaluated using different measurements covering various wavelength regimes. The analysis of electron density data, recorded on the ground and in the geospace at different latitudes, displayed power spectra with slopes ranging from 1.5 to 2.5 (Di Mare et al., 2021; Hobara et al., 2005; Jahn & Labelle, 1998; Kelley et al., 2002; Labelle et al., 1986; Spicher et al., 2014) although the most commonly reported value is around 1.9 (Basu et al., 1988; Kintner & Seyler, 1985; Tsunoda, 1988). The reason behind the large scatter in the spectral indices is not obvious. Probably an important role is played by the different regions of space where the data are recorded, by the instrumentation of satellites, rockets, and balloons used that may not be able to distinguish the dimensionality of the turbulent field (Pécseli, 2016) and by the range of the analyzed scale lengths. However, instability and turbulence processes certainly play an important role, but they are not the only processes responsible for the onset and evolution of plasma density irregularities (Materassi et al., 2020). For example, it has been suggested by Kelley et al. (1982) and later by Tsunoda (1988) that the structured soft-electron precipitation can be the cause of the large-scale plasma density irregularities (kilometric scales) at high latitude in the dayside and nightside auroral oval and that these irregularities are convectively transported over great distances throughout the polar ionosphere by large electric fields. The small-scale irregularities would be the result of the development of instabilities acting on the steep gradients associated with these large-scale irregularities.

In the past, many studies related to plasma density irregularities were carried out using data recorded by ground-based instruments or instruments installed on board rockets and satellites (Basu et al., 1988; Dyrud et al., 2006). Recently, interesting results have been obtained by analyzing measurements from the European Space Agency (ESA) Swarm constellation (Friis-Christensen et al., 2008), which consists of three identical satellites flying around the Earth in a near-polar orbit at two different altitudes, that is, around 460 and 50 km above. Measurements of magnetic field (see, e.g., De Michelis et al. (2019) and references therein) and electron density (De Michelis, Consolini, Pignalberi, et al., 2021; De Michelis, Consolini, Tozzi, et al., 2021), along the orbits of Swarm satellites, have been used to address the scaling properties of their fluctuations and to unveil some interesting features of ionospheric dynamics. These studies have demonstrated the existence of a class of plasma density irregularities characterized by both fluctuations and an energy spectrum supporting the role of turbulent processes at their origin. In addition, these studies also showed that this class is always associated with very high values of the Rate Of change of electron Density Index (RODI), which is a proxy of the fluctuations intensity characterizing the ionospheric medium. This implies that, among all the possible ionospheric irregularities, those due to turbulent processes seem to be always accompanied by plasma density variations stronger than those generated by other mechanisms. This last feature is independent of both latitude and geomagnetic activity.

In this work, we use data recorded on board two of the three satellites of the Swarm constellation (namely, Swarm A and Swarm B) to assess the possible dependence of the GPS signals LoL on the presence of a specific kind of ionospheric irregularities, and thereby to shed some light on the possible origin of one of the largest space

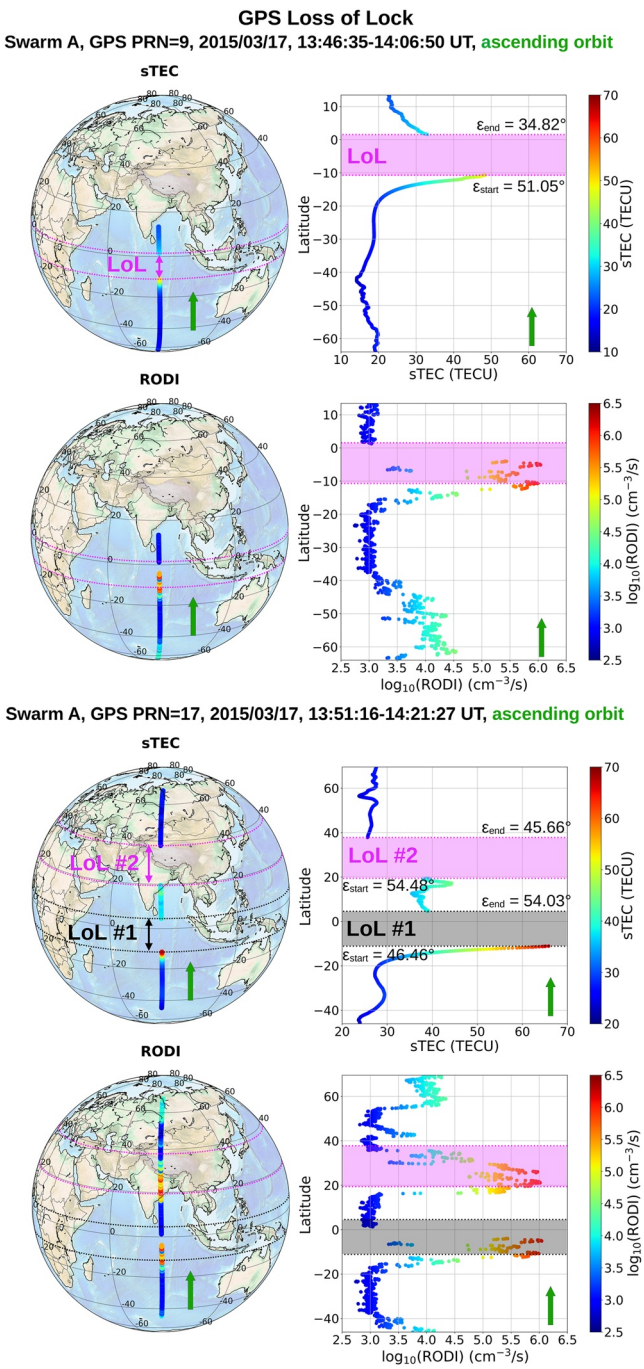

Figure 1. Examples of Global Positioning System loss of lock (GPS LoL) events as identified on 17 March 2015 in the slant TEC (sTEC) time series measured by Swarm A during the same orbit (the green arrow indicates whether the orbit is ascending or descending), but related to different satellites, Pseudo Random Noise number (PRN) = 9 (top) and PRN = 17 (bottom), and corresponding Rate Of change of electron Density Index (RODI) values calculated from electron density measurements. The magenta and gray belts identify the GPS LoL duration. Left panels represent the satellite track in a geographic coordinates map, while right panels show the corresponding plot latitude versus value (sTEC or RODI). The sTEC plot shows also the elevation angle of the satellite at the start (ϵ_{start}) and at the end (ϵ_{end}) of the LoL event.

weather effects on GNSS. Our results show that plasma density irregularities in a turbulent state characterized by intermittent structures and extremely high values of RODI can lead to GPS LoL events.

2. Data

In this study, we consider measurements from the Langmuir probes (Knudsen et al., 2017) and the precise orbit determination (POD) antennas (van den IJssel et al., 2015) on board Swarm A and Swarm B. These satellites were launched on 22 November 2013 in a circular near-polar orbit and are still operating. Their inclination is between 87° and 88° while the initial altitudes were about 460 km for Swarm A and 510 km for Swarm B. In detail, we use electron density (N_e) measurements collected by the Langmuir probes and Swarm Level-2 Total Electron Content (TEC) data, which contain time series of vertical and slant (both absolute and relative) TEC relative to each GPS satellite in view. Data are relative to a period of about 90 months, from 15 July 2014 to 31 December 2021, have a time resolution of 1 Hz, and can be downloaded from the ESA dissemination server (ftp://swarm-diss.eo.esa.int). Using N_e time series it is possible to calculate RODI, which is the standard deviation of N_e time derivative calculated on a window of fixed width sliding along N_e time series. In detail, RODI is defined as

$$\mathrm{RODI}(t) = \sqrt{\frac{1}{N-1}\sum_{t_i=t-\frac{\Delta t}{2}}^{t_i=t+\frac{\Delta t}{2}}\left(\mathrm{ROD}(t_i) - \overline{\mathrm{ROD}(t)}\right)^2}, \tag{1}$$

where ROD (Rate Of change of electron Density) is the time derivative of the electron density recorded at time t, and $\overline{\mathrm{ROD}(t)}$ is the corresponding arithmetic mean in the sliding window. The width of the sliding window used for RODI calculation is $\Delta t = 10$ s, and due to the 1-Hz sampling rate of N_e data, the number of values falling in the window is therefore $N = 11$. For further info on RODI calculation from Swarm N_e data, please refer to Pignalberi (2021).

In order to identify a GPS LoL we use the Swarm Level-2 slant TEC (sTEC) time series. These are calculated from L_1 and L_2 ambiguity-corrected carrier phase observations contained in the RINEX files from POD antennas. Evidently, the sTEC value cannot be calculated whenever L_1 and/or L_2 are unavailable and this can happen when either the GPS satellite is outside the field of view of POD antenna, or a LoL is ongoing. Thus, we identify the LoL events by looking for interruptions in the sTEC time series for a specific GPS satellite, which is identified by the corresponding Pseudo Random Noise number (PRN). We choose for interruptions a length from 1 to 1,200 s, that guarantees that the identified interruptions are actually LoL and not due to the fact that the satellite has gone out of the field of view (Pezzopane et al., 2021).

Figure 1 shows an example of LoL events recorded on board Swarm A during the St. Patrick storm occurred in March 2015. Specifically, the ascending orbit on 17 March 2015 between 13:46:35 and 14:06:50 UT and between 13:51:16 and 14:21:27 UT, related respectively to satellite PRN = 9 and satellite PRN = 17, is shown. Figure 1 points out that for PRN = 9, sTEC cannot be calculated in one segment of the orbit, while concerning PRN = 17 sTEC cannot be calculated in two segments of the orbit, because of LoL events occurring between the GPS receiver on board Swarm A and satellites.

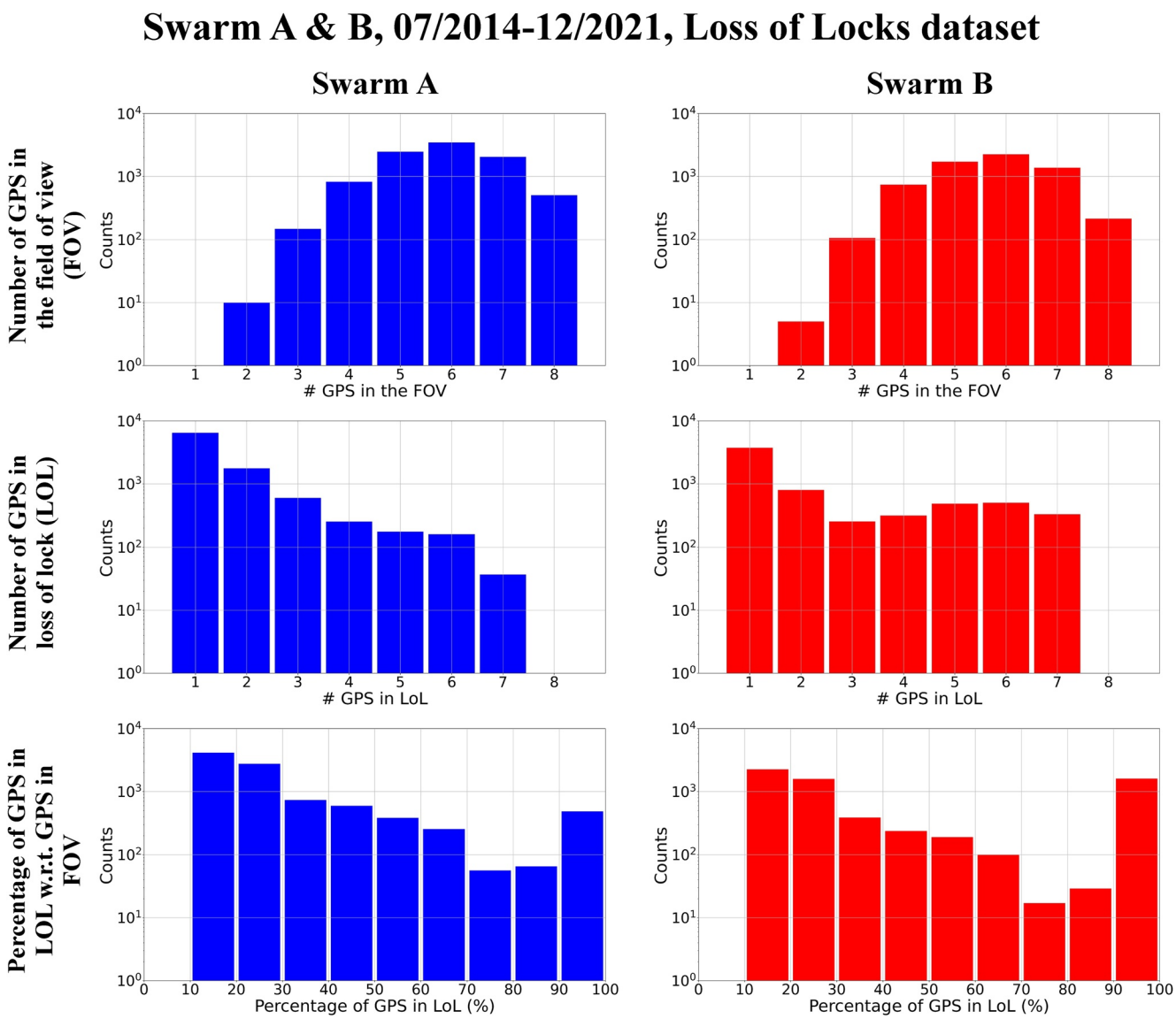

Figure 2. Loss of Lock statistics for Swarm A (left) and Swarm B (right) in terms of number of Global Positioning System (GPS) satellites in the field of view (top), number of GPS satellites in loss of lock (middle), and percentage of GPS satellites in loss of lock (bottom).

It is worth underlining that RODI, shown for the same orbit, significantly increases during the LoL events. This is an important aspect of the study because it testifies the fact that the irregularities responsible for the occurrence of the LoL event are close to the Swarm satellite. The same happens also for PRN = 1, PRN = 6, PRN = 7, PRN = 28 and PRN = 30 (corresponding figures can be found in the Supporting Information S1). By examining all the GPS LoL events recorded on board Swarm A and Swarm B satellites from 15 April 2014 to 31 December 2021, we have found that LoL events have different duration: from a few tens of seconds down to a single second. However, a check of LoL events whose duration is 1 s, evidenced that most of them are most likely not real (Pezzopane et al., 2021). This is the reason why we removed them from our initial data set and analyzed only all the observed events longer than 1 s. Figure 2 reports a LoL statistics showing the number of GPS satellites in the field of view, and the corresponding number and percentage of GPS satellites experiencing LoLs. Figure 3 shows instead the spatial occurrence of LoL events recorded on board Swarm A and Swarm B during the selected period. Most events cluster, in both hemispheres, at low and high latitudes, and their occurrence maximizes along the crests of the equatorial anomaly at low latitudes, and inside the auroral oval at high latitudes. It is worth highlighting that, even though the used LoL identification method is based on sTEC time series and not on carrier phase and pseudo-range time series as done by Xiong et al. (2016); Xiong et al. (2018), the distributions shown in Figure 3

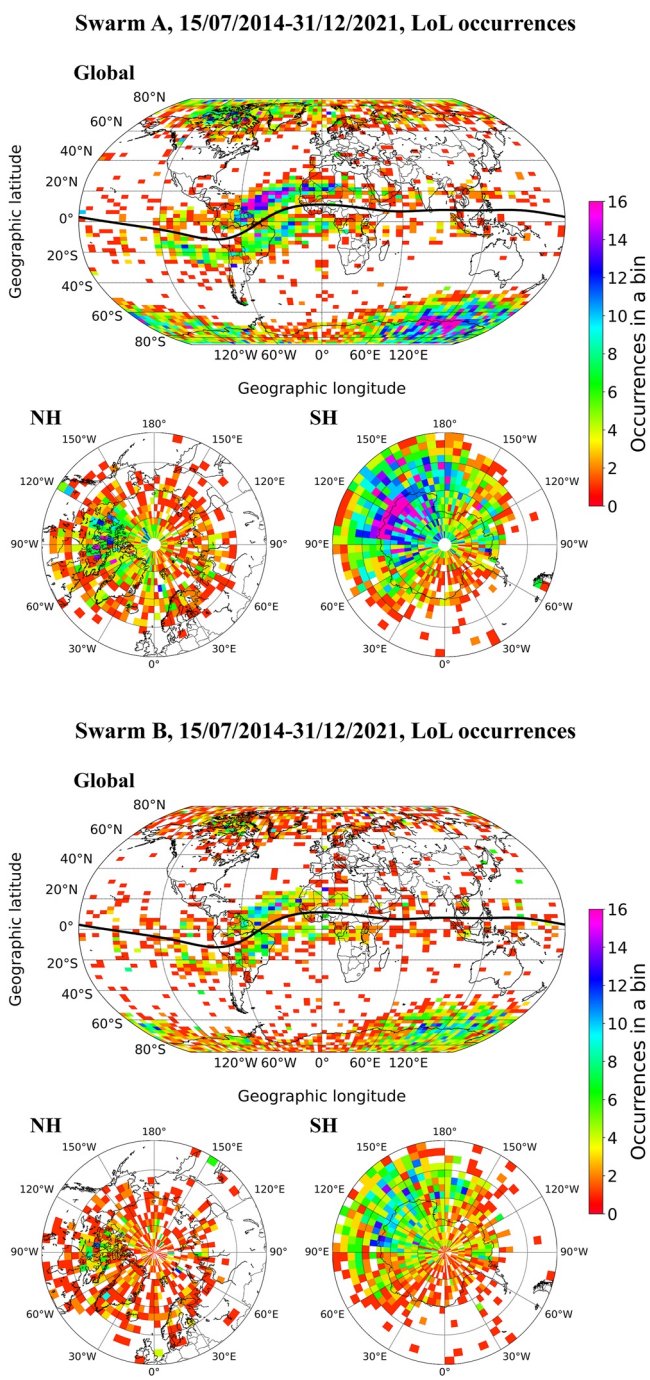

Figure 3. Geographic distribution of Global Positioning System loss of lock (LoL) occurrence for Swarm A and Swarm B, from 15 July 2014 to 31 December 2021, as global projection and as Northern hemisphere (from 50° N to the North pole) and Southern hemisphere (from 50°S to the South pole) polar projections, respectively. Bins are 2.5° wide in latitude, and 5° wide in longitude. The black curve in the global projection represents the magnetic equator.

are highly comparable with those found by Xiong et al. (2018). In addition, according to Xiong et al. (2016) also our analysis results in a lower number of LoL events for Swarm B than for Swarm A, suggesting that the higher you go, the more irregularities decrease in number. This is consistent with the fact that the plasma environment here investigated is the topside ionosphere where the electron density undergoes a nearly-exponential decrease with altitude. Indeed, at Swarm altitudes, the ionospheric plasma scale height is of the order or 50–100 km depending on latitude, local time, season, and solar activity (e.g., Pezzopane and Pignalberi (2019); Pignalberi et al. (2022)). This means that at the altitude of Swarm B, which flies about 50 km above Swarm A, the electron density is significantly reduced. More in general, after three scale heights (150–300 km) the electron density is reduced by a factor $1/e^3 \sim 0.05$, which reasonably suggests that 95% of the topside electron density is concentrated in a narrow range of altitudes above Swarm satellites and not much further away.

3. Method

One of the most striking features of turbulent signals is the scale-invariant character of their fluctuations, which implies the absence of a characteristic scale for the emerging fluctuation structures, that is, the occurrence of self-similarity/self-affinity in a statistical sense. A simple way to investigate the occurrence of scaling features in a time series is the evaluation of the so-called generalized qth-order structure function S_q (Frisch, 1995). It is defined as:

$$S_q(t) = \langle |f(t+\delta t) - f(t)|^q \rangle, \tag{2}$$

where $f(t)$ is the time series, δt is the temporal increment, and $\langle \ldots \rangle$ stands for a statistical mean. In the case of scale-invariant signals, the qth-order structure function is expected to scale as follows:

$$S_q(t) = \delta t^{\gamma(q)}, \tag{3}$$

where $\gamma(q)$ is the qth-order scaling exponent. Studying the structure function of a given signal is equivalent to study the scaling features of the moments of the distribution of its temporal increments at different temporal scales. The final goal is to compute a hierarchy of scaling indices, $\gamma(q)$, which characterizes the scaling features of the different moments of the signal increments (self-affinity of the signal). The first-order scaling exponent, $\gamma(1)$, also known as Hurst exponent, quantifies the persistent ($\gamma(1) > 0.5$) or anti-persistent ($\gamma(1) < 0.5$) character of the fluctuations, while the second-order scaling exponent, $\gamma(2)$, provides information on spectral features of the fluctuations, being the two quantities related via the Wiener-Khinchin theorem (Wiener, 1964). Indeed, the scaling exponent of the second-order structure function is directly related to the one of the power spectral density, PSD, (the Fourier transform of the auto-correlation function) through the following relation: $\beta = \gamma(2) + 1$, being β the power spectral exponent $S_q(f) \sim f^{-\beta}$. Here, to evaluate the local scaling features we use the Detrended Structure Function Analysis (DSFA) method (De Michelis et al., 2015), which has been successfully applied to investigate the local scaling features of both the electron density (see, e.g., Giannattasio et al. (2019)) and magnetic field fluctuations (see, e.g., De Michelis et al. (2017) and references therein) recorded on board Swarm constellation. In order to remove the long-scale variations that could prevent the correct estimation of the scaling features, this method departs from the traditional Detrended Fluctuation Analysis (Peng et al., 1994)

and joins the structure function analysis, traditionally used in turbulence studies, with a detrending function. The DSFA method is based on the evaluation of local scaling exponents within moving windows by using the structure function analysis applied to locally detrended time series. In our case, we consider a window of 301 points and evaluate, for each window, the structure function of the electron density. In this way, we are able to extract the scaling features of the electron density fluctuations on a local basis, namely the first and second-order scaling exponents. This is a fundamental point if we consider that the satellite crosses regions where different physical processes changing in space and time occur. To set a window of 301 points means to analyze the features of electron density fluctuations in a spatial range about 2,400 km-wide, being the orbital speed of Swarm constellation of about 8 km/s. Within each window, we investigate time increments, δt, ranging from 1 to 40 s, and associate the estimated scaling exponents with the position of the satellite corresponding to the center of the considered time window. Under the hypothesis that the transit time of the structure under observation is faster than its evolution (Taylor, 1938), the analysis of the time increments from 1 to 40 s corresponds to the analysis of spatial increments from 8 to 320 km. This means that we can study the features of the electron density fluctuations occurring in the meso-scale domain (i.e., from tens to hundreds of km) that is a particularly interesting domain where several processes and phenomena, typical of the high- and low-latitude ionosphere, occur. Indeed, at these scales some processes and/or phenomena as polar cap patches, blobs, auroral arcs, field aligned currents and plasma bubbles can be observed.

4. Results

Once LoL events have been identified in time and space, as it was described in Section 2, it is possible to investigate what are the features of the ionospheric environment that favor their occurrence. To accomplish this task, we consider all the start times of LoL events longer than 1 s and analyze the corresponding local fluctuation scaling properties of the electron density measurements. Specifically, the local scaling properties concern the behavior of a structure, that is, an irregularity in this case, as a function of the scale at which it is viewed. These features are essential to understand and characterize the complexity of the structure (Schmitt & Huang, 2016). In our case, they allow us to capture some peculiar features of the local electron density fluctuations and shed light on the so-called multiscale dynamics, which characterizes all those complex systems in which a large range of time and/or spatial scales may interact with each other. The local scaling properties (as inferred from structure function analysis), for example, provide information on the persistent or anti-persistent nature of the fluctuations and indirectly on their spectral features. From the presence of persistence or anti-persistence it is possible to infer some important aspects of the dynamical physical processes at the origin of the observed electron density fluctuations. Fluctuations with a persistent character are typical of systems with a long-range dependence, for which we can suppose long-term memory effects of the fluctuations sign. Conversely, fluctuations with an anti-persistent character exhibit higher noise and more volatility. This means that persistent fluctuations can be associated with the formation of large-scale density structures, while anti-persistent fluctuations can be associated with small-scale density structures. From the knowledge of the local scaling properties, it is also possible to indirectly infer the spectral features of the analyzed time series. These, in turn, allow discriminating among the different kinds of instabilities or turbulent processes that originated the observed fluctuations. For example, slopes of the power spectrum ranging between $-5/3$ and -3 are associated with different turbulent regimes like, for example, the shear-flow turbulence with a direct or an inverse energy cascade, the turbulence driven by the $\vec{E} \times \vec{B}$ convective instability, or the turbulence driven by strong electron density gradient drifts (Kintner & Seyler, 1985). Since LoL events are mainly located in two specific regions (equatorial and polar), the analysis is limited to two well-defined regions: (a) the mid- and high-magnetic latitudes ($|\mathrm{QDLat}| > 50°$; QDLat being latitude in the quasi-dipole (QD) coordinate system (Emmert et al., 2010)), without distinguishing the Northern hemisphere from the Southern one; (b) the equatorial belt ($|\mathrm{QDLat}| < 30°$).

Figure 4 displays the joint probability density function (PDF) of RODI and the first- and second-order scaling exponents conditioned to the occurrence of LoL events at mid and high latitudes, analyzing Swarm A and Swarm B separately, and considering only the points at which LoL events start. The figure shows that the two conditioned PDFs are very similar to each other, as also confirmed by Figure 5, where the conditioned PDFs shown in Figure 4 are overlapped. Thus, at mid and high latitudes the features of electron density fluctuations associated with LoL events do not seem to be affected by the altitude difference (~50 km) between the orbits of the two satellites. By virtue of this, we decided to merge the two datasets of Swarm A and B, and Figure 6

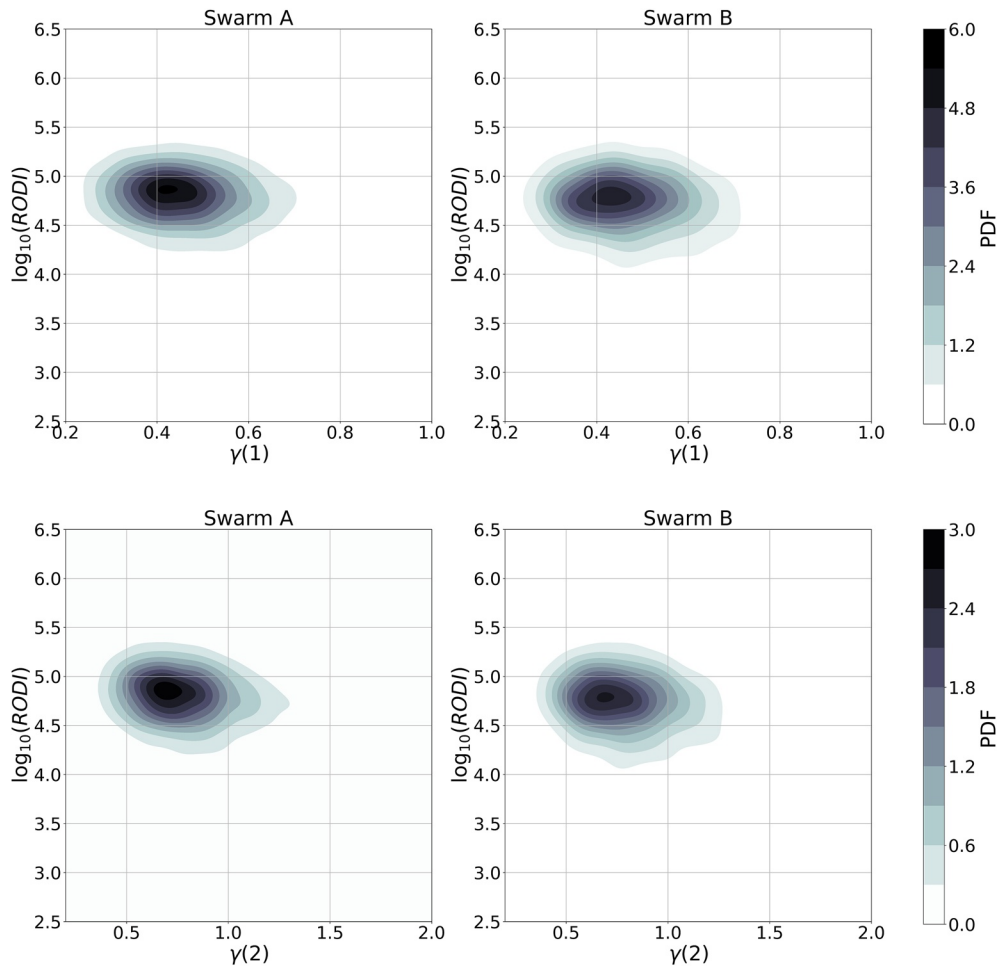

Figure 4. Conditioned joint probability density function (PDF) of Rate Of change of electron Density Index (RODI) and $\gamma(1)$ (top panels) and $\gamma(2)$ (bottom panels) analyzing Swarm A and Swarm B separately. Data refer to mid and high latitudes ($|QDLat| > 50°$) and are those calculated simultaneously to the occurrence of Global Positioning System loss of lock events. QDLat is the latitude in the quasi-dipole coordinate system.

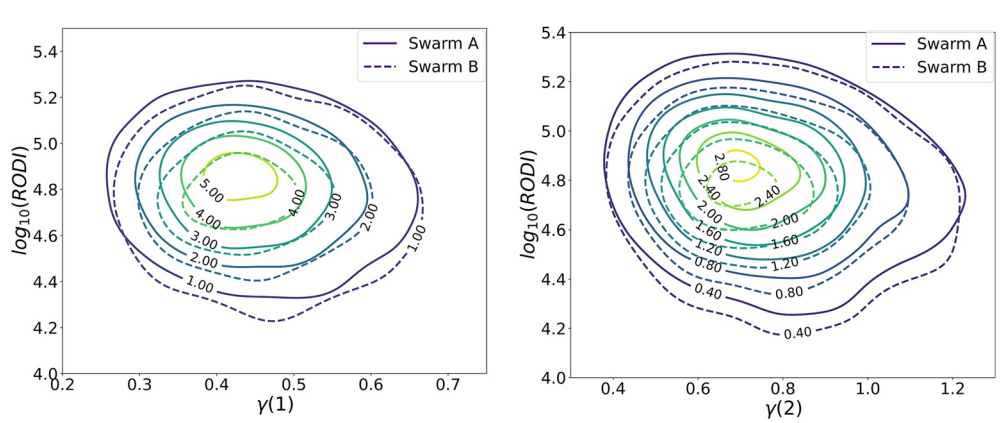

Figure 5. Overlap of the conditioned joint probability density functions of Rate Of change of electron Density Index (RODI) and $\gamma(1)$ (left panel) and $\gamma(2)$ (right panel), evaluated using Swarm A and Swarm B data, shown separately in Figure 4.

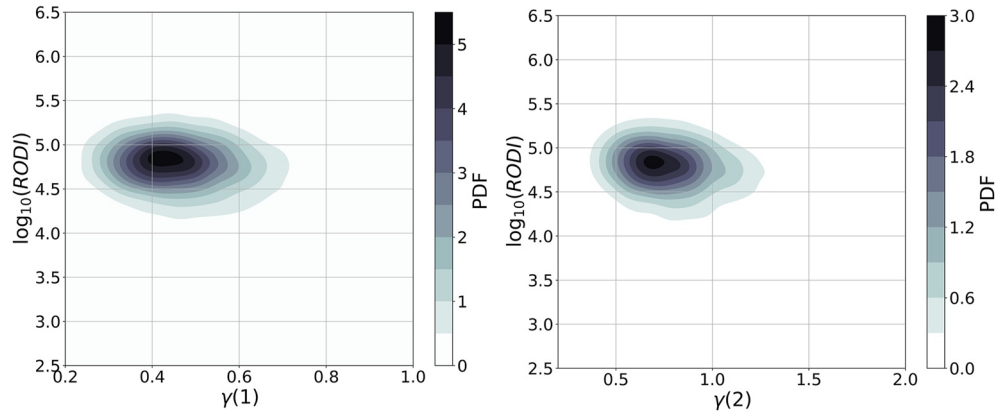

Figure 6. Conditioned joint probability density functions (PDF) of Rate Of change of electron Density Index (RODI) and $\gamma(1)$ (left panel) and $\gamma(2)$ (right panel) for the joint data set (Swarm A + Swarm B). Data refer to mid and high latitudes (|QDLat| > 50°) and are those calculated simultaneously to the occurrence of Global Positioning System loss of lock events. QDLat is the latitude in the quasi-dipole coordinate system.

reports the analysis already shown in Figure 4 but carried out on the joint data set. The conditioned PDFs of RODI and the first- and second-order scaling exponents show that GPS LoL events are mainly associated with $\gamma(1) = (0.47 \pm 0.12)$, $\gamma(2) = (0.8 \pm 0.2)$, and RODI > 10^4(cm^{-3} s^{-1}).

The same analysis is applied to the equatorial belt (|QDLat| < 30°). Figure 7 reports the conditioned PDFs of RODI and the first- and second-order scaling exponents obtained considering the two satellites separately, that are overlapped in Figure 8. Also in this case the altitude difference (~50 km) between the orbits of the two satellites does not affect the results, so Figure 9 reports the analysis already shown in Figure 7 but performed on the joint data set. In this case, differently from the case of mid and high latitudes, electron density fluctuations are mainly characterized by a mean value of the first-order scaling exponent $\gamma(1) = (0.64 \pm 0.13)$, suggesting a more persistent character of the fluctuations, and by a mean value of the second-order scaling exponent $\gamma(2) = (1.0 \pm 0.2)$. In this case, RODI values are extremely high, even higher than those obtained for mid and high latitude regions. However, there is also an additional class of events for which the electron density fluctuations show completely different properties: RODI < $10^{3.5}$ cm^{-3} s^{-1}, $\gamma(1) > 0.6$, and $\gamma(2) > 1$. This class consists of nearly 25% of all recorded events and the values of the scaling exponents associated with the electron density fluctuations suggest a different origin for the LoL of the GPS signals.

To better characterize this additional class of events we introduce a pseudo-intermittency parameter (μ) (briefly called intermittency in the following), capable of giving us information on the occurrence of anomalous scaling features, that is, on the departure from a linear trend of the scaling exponents $\gamma(q)$ on moment order q. This pseudo-intermittency parameter, μ, is defined according to the following expression,

$$\mu = \gamma(1) - 2\gamma(2), \tag{4}$$

so that it is a measure of how the scaling exponents ($\gamma(1)$ and $\gamma(2)$) depart from a linear dependence on q. If $\mu > 0$, then the trend of $\gamma(q)$ is convex. This is exactly what is observed for the occurrence of intermittency in turbulence (Frisch, 1995) and is an evidence of a multifractal character of the cascading process (i.e., the energy transfer among the scales). Furthermore, the greater the value of intermittency, the greater the non-homogeneity with which the energy is redistributed at all the time and/or spatial scales. Figure 10 reports the conditioned joint PDF of RODI and pseudo-intermittency (μ) during GPS LoL events considering the joint data set (Swarm A + Swarm B) for both mid and high latitudes (left panel) and the equatorial belt (right panel). At mid and high latitudes the plasma density irregularities associated with GPS LoL events are in a turbulent state always characterized by a certain degree of intermittency. Conversely, in the equatorial belt there are two different families of irregularities associated with GPS LoL events, characterized by significantly different values of intermittency. The plasma density irregularities with higher intermittency values are also characterized by extremely high values of RODI and $\gamma(2)$ around 1, as can be seen from the three-dimensional plot of Figure 11. Therefore, as it happens at high

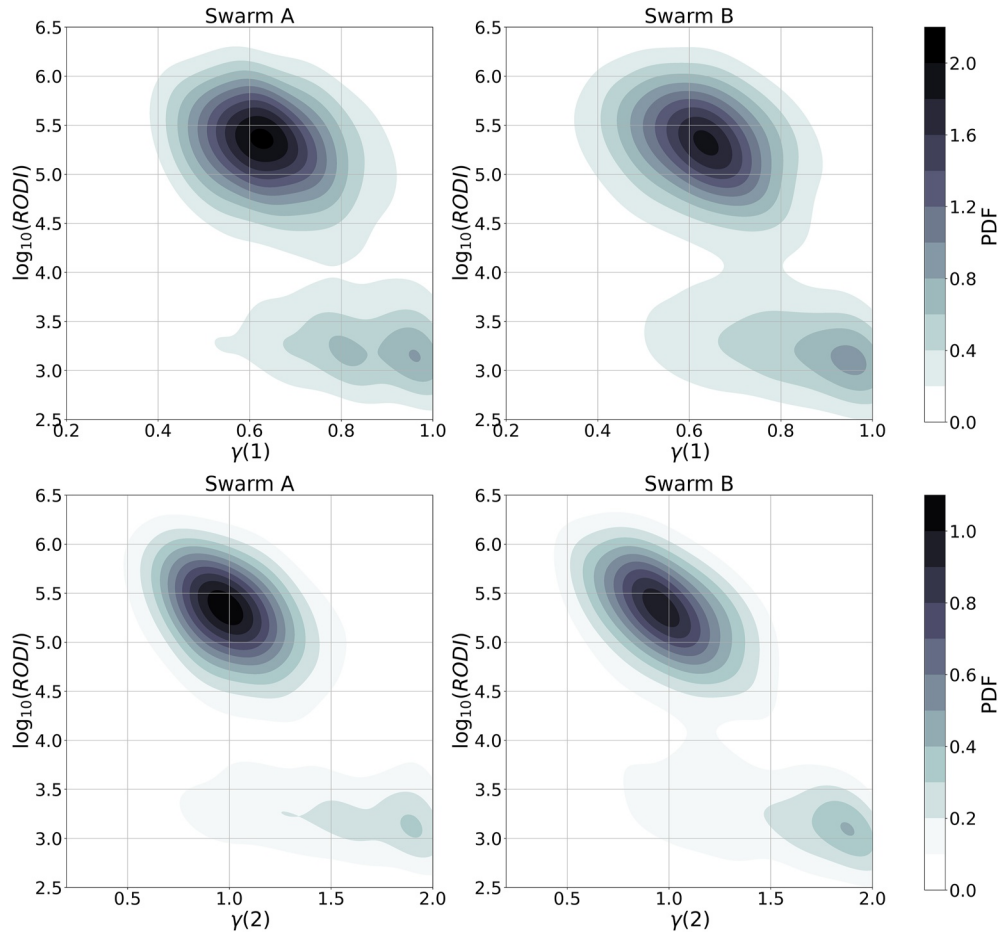

Figure 7. Conditioned joint probability density functions (PDF) of Rate Of change of electron Density Index (RODI) and $\gamma(1)$ (top panels) and $\gamma(2)$ (bottom panels) analyzing Swarm A and Swarm B separately. Data refer to the equatorial belt ($|QDLat| < 30°$) and are those calculated simultaneously to the occurrence of Global Positioning System loss of lock events. QDLat is the latitude in the quasi-dipole coordinate system.

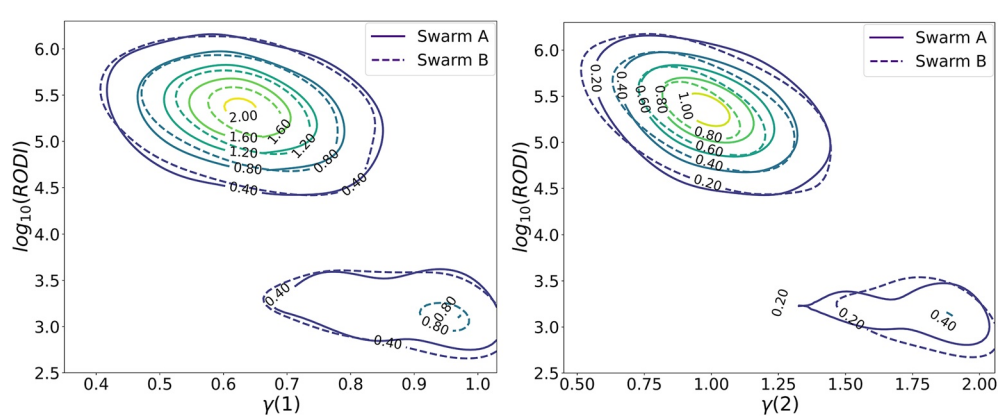

Figure 8. Overlapping of the conditioned joint probability density functions of Rate Of change of electron Density Index (RODI) and $\gamma(1)$ (left panel) and $\gamma(2)$ (right panel), evaluated using Swarm A and Swarm B data, shown separately in Figure 7.

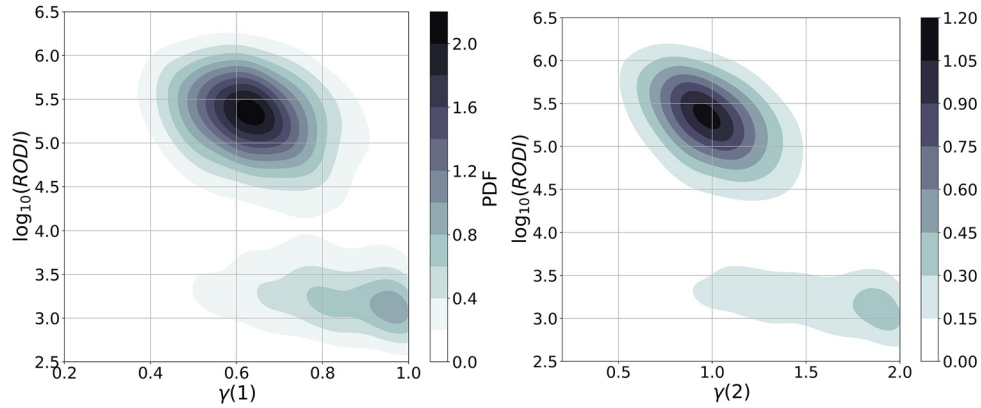

Figure 9. Conditioned joint probability density functions (PDF) of Rate Of change of electron Density Index (RODI) and $\gamma(1)$ (left panel) and $\gamma(2)$ (right panel) considering the joint data set (Swarm A + Swarm B). Data refer to the equatorial belt (|QDLat| < 30°) and are those calculated simultaneously to the occurrence of Global Positioning System loss of lock events. QDLat is the latitude in the quasi-dipole coordinate system.

latitudes, also in the equatorial belt, plasma density irregularities with extremely high values of RODI are in a intermittent turbulent state.

5. Discussion and Conclusions

Recently, by analyzing the scaling properties of some ionospheric parameters, De Michelis, Consolini, Pignalberi, et al. (2021) and De Michelis, Consolini, Tozzi, et al. (2021) identified two distinct classes of plasma density fluctuations in the ionosphere characterized by different mean values of both the scaling exponents and RODI. Specifically, one of these two classes shows a second-order scaling exponent $\gamma(2) \leq 1$ and extremely high values of RODI (typically, larger than $10^{3.5}$ cm^{-3} s^{-1}). At high latitudes, this class is mainly located inside the auroral oval (De Michelis, Consolini, Pignalberi, et al., 2021; De Michelis et al., 2020). In the equatorial regions, it essentially coincides with the so-called plasma bubbles (De Michelis, Consolini, Tozzi, et al., 2021), that is, electron density irregularities produced after sunset by the nonlinear evolution of the Rayleigh–Taylor instability (Kelley, 2009). The scaling properties of the electron density fluctuations of this class suggest their possible turbulent state, that is the existence of multiscale fluctuations, which occur over a very wide range of spatial and temporal scales, due to a continuous transfer of energy from the injection scales to the dissipation ones. Here, we investigate whether the GPS LoL events are somehow linked to this specific class of electron density fluctuations.

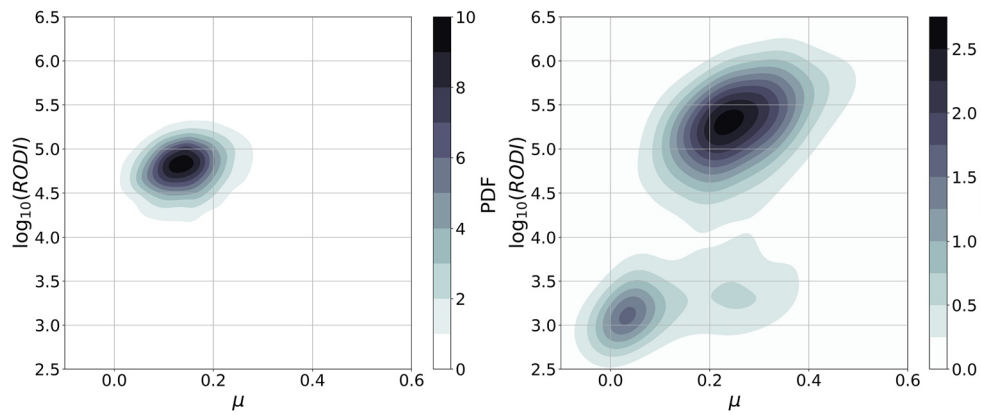

Figure 10. Conditioned joint probability density functions (PDF) of Rate Of change of electron Density Index (RODI) and intermittency (μ) at mid and high latitude regions (left panel) and equatorial belt (right panel) during Global Positioning System loss of lock events considering the joint data set (Swarm A + Swarm B).

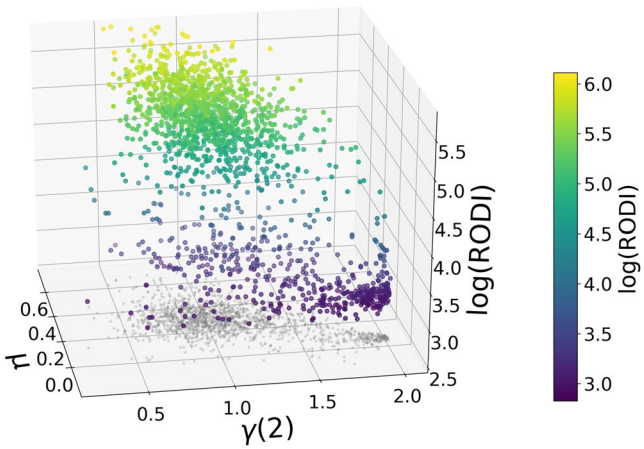

Figure 11. Rate Of change of electron Density Index (RODI), intermittency parameter (μ) and second-order scaling exponent ($\gamma(2)$) values of plasma density irregularities during Global Positioning System loss of lock events in the equatorial belt (|QDLat| < 30°). QDLat is the latitude in the quasi-dipole coordinate system. The joint data set (Swarm A + Swarm B) is considered.

Figure 12 reports a comparison between the features of electron density fluctuations corresponding to the GPS LoL events, as reported in Figure 6, for mid and high latitudes and those obtained by considering all the available electron density data recorded in the same regions and for the same period according to De Michelis, Consolini, Pignalberi, et al. (2021). We note that the occurrence of GPS LoL events is associated with the specific class of electron density fluctuations, showing a second-order scaling exponent $\gamma(2) \leq 1$ and extremely high values of RODI. In addition, RODI seems to be a proxy of this class: values of Log (RODI) > 4 are associated with the occurrence of LoL events.

Similar results are found also in the equatorial region and shown in Figure 13, which displays a comparison between the electron density fluctuation scaling properties associated to GPS LoL events, as reported in Figure 9, and those obtained in correspondence of plasma bubbles according to De Michelis, Consolini, Tozzi, et al. (2021). These authors showed that plasma bubbles are irregularities that present spectral features and RODI values that are significantly different from those characterizing the background environment where they develop. Specifically, they found that electron density fluctuations associated with plasma bubbles fall right into the class showing a second-order scaling exponent $\gamma(2) \leq 1$ and extremely high values of RODI. Figure 13 clearly highlights how, in the equatorial belt, the features shown by the electron density fluctuations associated with GPS LoL events are really similar to those of plasma bubbles. This suggests that in the equatorial ionosphere most of GPS LoL events are triggered by the plasma bubbles development. However, about 25% of the LoL events recorded in the equatorial belt do not seem to be related to the presence of plasma bubbles. They are characterized by electron density fluctuations with low RODI values (log(RODI) < 4) and different scaling properties. Figure 14 shows the distribution in the QDLat-MLT (magnetic local time) plane of these GPS LoL events (blue dots). The hours at which most of these events occur highlight that they are most likely related also to physical phenomena different from those at the base of the plasma bubbles development. In detail, only a small fraction of these events occur under conditions (MLT and QDLat values) compatible with the development of plasma bubbles, that are the occurrence in the post sunset sector and the appearance in a narrow latitudinal band centered over the magnetic equator of the Earth. Indeed, during the day, the high conductance of the E region relative to the F region prevents the appearance of plasma bubbles, which are generated by the transport of plasma from the bottomside to the topside ionosphere by the

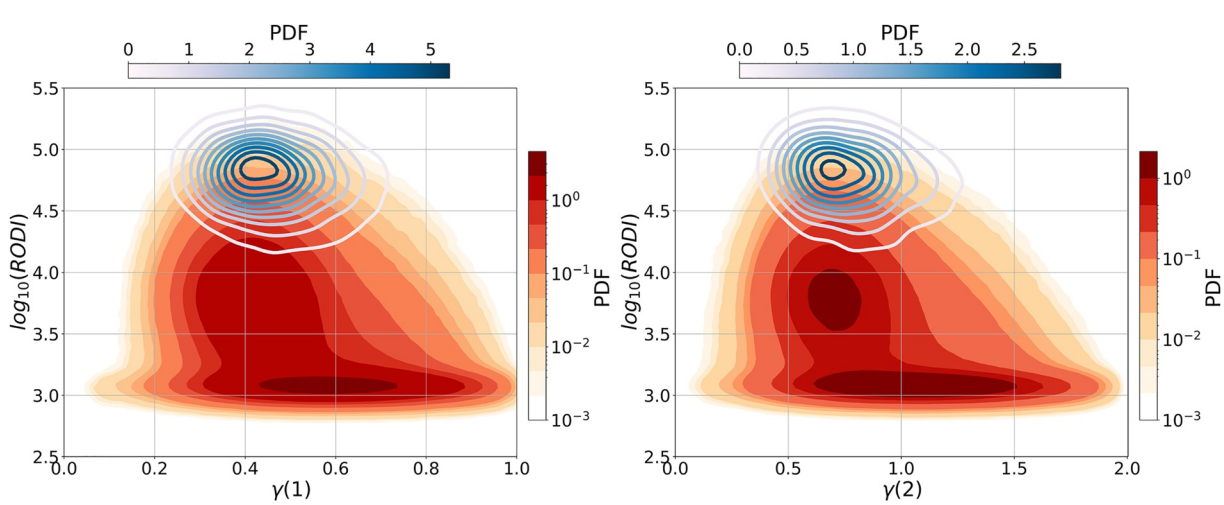

Figure 12. Conditioned joint probability density functions (PDF) of Rate Of change of electron Density Index (RODI) and $\gamma(1)$ (left panel) and $\gamma(2)$ (right panel) at mid- and high-latitude regions (|QDLat| > 50°) during Global Positioning System loss of lock (LoL) events (the same reported in Figure 6, here shown as blue-scale line contours) and the same quantity obtained considering all data and not only those corresponding to a LoL event (here shown as red-scale filled contours). QDLat is the latitude in the quasi-dipole coordinate system.

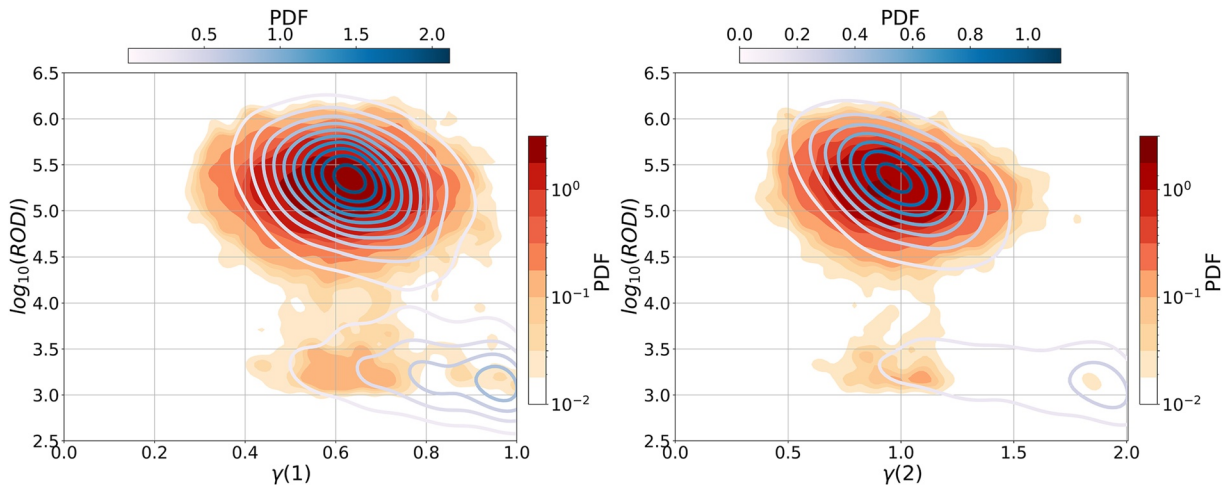

Figure 13. Conditioned joint probability density functions (PDFs) of Rate Of change of electron Density Index (RODI) and $\gamma(1)$ (left panel) and $\gamma(2)$ (right panel) at low latitude (|QDLat| < 30°) during Global Positioning System loss of lock events (the same reported in Figure 9, here shown as blue-scale contours) and the same quantity obtained considering plasma bubbles occurrence (here shown as red-scale filled contours). QDLat is the latitude in the quasi-dipole coordinate system.

generalized Rayleigh-Taylor instability. An hypothesis is that these GPS LoL events, associated with electron density fluctuations characterized by completely different scaling properties, are triggered by plasma blobs, that are mesoscale plasma density enhancements relative to the ambient plasma with longitudinal widths comparable to those of equatorial bubbles. These plasma density irregularities, unlike equatorial bubbles, are more frequently detected around ±20° – 30° magnetic latitudes (Choi et al., 2012; Haaser et al., 2012; Watanabe & Oya, 1986), although they can be also observed at night at low and mid latitudes in association with equatorial plasma bubbles (Martinis et al., 2009; Park et al., 2003; Yokoyama et al., 2007).

Moreover, our findings show that both the scaling exponent values corresponding with GPS LoL events in the two analyzed regions (mid and high latitudes and the equatorial belt) and the corresponding values of RODI depend on latitude, suggesting that the physical processes at the base of a GPS LoL event can change with the latitude. Indeed, the values of the second-order scaling exponents are slightly different moving from high to low latitudes. Furthermore, also the persistence character of the high/low-latitude fluctuations is different, being the first-order scaling exponent below 0.5 at high latitudes (anti-persistent fluctuations) and above 0.5 at low latitudes (persistent fluctuations). Another relevant feature is that generally $\gamma(2) < 2\gamma(1)$, that is $\mu > 0$, so that the dependence of the scaling exponents of the structure functions on the moment order q is expected to be concave, which could be an indication of a multifractal (intermittent) character of the density fluctuations. The different values of the first and second order scaling exponents at high and low latitudes suggest that different instability/turbulence processes can be at the origin of the ionospheric irregularities' generation. On the other hand, we know that, for example, the Rayleigh-Taylor instability plays a fundamental role at low latitudes (e.g., Kelley (2009)), while the gradient drift instability, the Kelvin-Helmholtz instability, the $\vec{E} \times \vec{B}$ instability and/or the drift wave turbulence, are processes essentially occurring at high latitudes (e.g., Tsunoda et al. (1985)). This could be the origin of the observed differences in the high-latitude and low-latitude scaling exponents values that characterize the electron density turbulent fluctuations during the GPS LoL events. Indeed, it has been suggested from theory and plasma simulations that different turbulence spectral indices can be associated with different density irregularities and mechanisms at their origin. For instance, Gruzinov et al. (1996) have shown that a two-dimensional $\vec{E} \times \vec{B}$ convective turbulence in the early phase displays spectral features similar to the ordinary fluid turbulence, that is, $\beta \simeq -5/3$, while at later stages the spectral features tend to display more steeper spectral exponents ($\beta \simeq -2$), and this could be the case of the plasma bubbles. Differently, gradient-drift/current-convective and Kelvin-Helmoltz instabilities are capable of generating turbulence

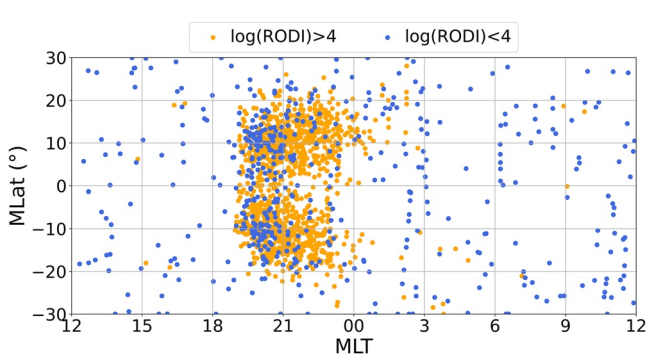

Figure 14. Low latitude (|QDLat| < 30°) distribution in the QDLat-magnetic local time (MLT) plane of Global Positioning System loss of lock events for Swarm A and Swarm B, from 15 July 2014 to 31 December 2021 according to different log (RODI) values. QDLat is the latitude in the quasi-dipole coordinate system.

spectra characterized by spectral exponents close to −5/3 in the case of direct and inverse cascade (Kintner & Seyler, 1985). This could be the case for the high-latitude region where the observed spectral features could be associated with irregularities as the plasma patches.

In conclusion, the main result of our study is that when a GPS LoL event is ongoing, electron density fluctuations are in a turbulent state characterized by intermittent structures and generally accompanied by extremely high values of RODI ($>10^4$ cm^{-3} s^{-1}). This is always the case at mid and high latitudes (|QDLat| > 50°), while in the equatorial belt this happens in at least 75% of GPS LOL events. This is a significant result that might help when implementing empirical models capable of identifying the regions where there are the physical conditions for the occurrence of disturbances potentially harmful to the propagation of radio signals.

Data Availability Statement

The results presented rely on data collected by ESA-Swarm mission. We thank the European Space Agency that supports the Swarm mission. Swarm data can be accessed at ftp://swarm-diss.eo.esa.int.

Acknowledgments
The authors acknowledge financial support from European Space Agency (ESA contract N. 4000125663/18/I-NB- "EO Science for Society Permanently Open Call for Proposals EOEP-5 BLOCK4" (INTENS)) and from Italian PNRA under contract PNRA18-00289-A "Space weather in Polar Ionosphere: the Role of Turbulence (SPIRiT)".

References

Basu, S., Basu, S., MacKenzie, E., Fougere, P. F., Coley, W. R., Maynard, N. C., et al. (1988). Simultaneous density and electric field fluctuation spectra associated with velocity shears in the auroral oval. *Journal of Geophysical Research*, *93*(A1), 115–136. https://doi.org/10.1029/JA093iA01p00115

Choi, H. S., Kil, H., Kwak, Y. S., Park, Y. D., & Cho, K. S. (2012). Comparison of the bubble and blob distributions during the solar minimum. *Journal of Geophysical Research*, *117*(A4), A04314. https://doi.org/10.1029/2011JA017292

De Michelis, P., Consolini, G., Pignalberi, A., Tozzi, R., Coco, I., Giannattasio, F., et al. (2021). Looking for a proxy of the ionospheric turbulence with Swarm data. *Scientific Reports*, *11*(1), 6183. https://doi.org/10.1038/s41598-021-84985-1

De Michelis, P., Consolini, G., & Tozzi, R. (2015). Magnetic field fluctuation features at Swarm's altitude: A fractal approach. *Geophysical Research Letters*, *42*(9), 3100–3105. https://doi.org/10.1002/2015GL063603

De Michelis, P., Consolini, G., Tozzi, R., Giannattasio, F., Quattrociocchi, V., & Coco, I. (2019). Features of magnetic field fluctuations in the ionosphere at Swarm altitude. *Annals of Geophysics*, *62*(4). https://doi.org/10.4401/ag-7789

De Michelis, P., Consolini, G., Tozzi, R., & Marcucci, M. F. (2017). Scaling Features of High-Latitude Geomagnetic Field Fluctuations at Swarm Altitude: Impact of IMF Orientation. *Journal of Geophysical Research*, *122*(10), 10548–10562. https://doi.org/10.1002/2017JA024156

De Michelis, P., Consolini, G., Tozzi, R., Pignalberi, A., Pezzopane, M., Coco, I., et al. (2021). Ionospheric turbulence and the equatorial plasma density irregularities: Scaling features and RODI. *Remote Sensing*, *13*(4), 759. https://doi.org/10.3390/rs13040759

De Michelis, P., Pignalberi, A., Consolini, G., Coco, I., Tozzi, R., Pezzopane, M., et al. (2020). On the 2015 St. Patrick's storm turbulent state of the ionosphere: Hints from the Swarm mission. *Journal of Geophysical Research*, *125*(8), e27934. https://doi.org/10.1029/2020JA027934

Di Mare, F., Spicher, A., Clausen, L. B. N., Miloch, W. J., & Moen, J. I. (2021). Turbulence and Intermittency in the Winter Cusp Ionosphere Studied With the ICI Sounding Rockets. *Journal of Geophysical Research*, *126*(8), e29150. https://doi.org/10.1029/2021JA029150

Dyrud, L., Krane, B., Oppenheim, M., Pécseli, H. L., Schlegel, K., Trulsen, J., & Wernik, A. W. (2006). Low-frequency electrostatic waves in the ionospheric E-region: A comparison of rocket observations and numerical simulations. *Annales Geophysicae*, *24*(11), 2959–2979. https://doi.org/10.5194/angeo-24-2959-2006

Emmert, J. T., Richmond, A. D., & Drob, D. P. (2010). A computationally compact representation of Magnetic-Apex and Quasi-Dipole coordinates with smooth base vectors. *Journal of Geophysical Research*, *115*, A08322. https://doi.org/10.1029/2010JA015326

Friis-Christensen, E., Lühr, H., Knudsen, D., & Haagmans, R. (2008). Swarm an Earth observation mission investigating geospace. *Advances in Space Research*, *41*(1), 210–216. https://doi.org/10.1016/j.asr.2006.10.008

Frisch, U. (1995). *Turbulence: The legacy of a. n. Kolmogorov*. Cambridge University Press. https://doi.org/10.1017/CBO9781139170666

Giannattasio, F., De Michelis, P., Consolini, G., Quattrociocchi, V., Coco, I., & Tozzi, R. (2019). Characterising the electron density fluctuations in the high-latitude ionosphere at Swarm altitude in response to the geomagnetic activity. *Annals of Geophysics*, *62*(4). https://doi.org/10.4401/ag-7790

Gruzinov, A. V., Kukharkin, N., & Sudan, R. N. (1996). Two-dimensional convective turbulence. *Physical Review Letters*, *76*(8), 1260–1263. https://doi.org/10.1103/PhysRevLett.76.1260

Haaser, R. A., Earle, G. D., Heelis, R. A., Klenzing, J., Stoneback, R., Coley, W. R., & Burrell, A. G. (2012). Characteristics of low-latitude ionospheric depletions and enhancements during solar minimum. *Journal of Geophysical Research*, *117*(A10), A10305. https://doi.org/10.1029/2012JA017814

Hobara, Y., Lefeuvre, F., Parrot, M., & Molchanov, O. A. (2005). Low-latitude ionospheric turbulence observed by Aureol-3 satellite. *Annales Geophysicae*, *23*(4), 1259–1270. https://doi.org/10.5194/angeo-23-1259-2005

Hysell, D. L., & Shume, E. B. (2002). Electrostatic plasma turbulence in the topside equatorial F region ionosphere. *Journal of Geophysical Research*, *107*(A10), 1269. https://doi.org/10.1029/2001JA000227

Jahn, J.-M., & Labelle, J. (1998). Rocket measurements of high-altitude spread F irregularities at the magnetic dip equator. *Journal of Geophysical Research*, *103*(A10), 23427–23442. https://doi.org/10.1029/97JA02636

Kelley, M. C. (2009). The Earth's ionosphere: Plasma physics and electrodynamics (2nd ed.).

Kelley, M. C., Franz, T. L., & Prasad, G. (2002). On the turbulent spectrum of equatorial spread F: A comparison between laboratory and space results. *Journal of Geophysical Research*, *107*(A12), 1432. https://doi.org/10.1029/2002JA009398

Kelley, M. C., Vickrey, J. F., Carlson, C. W., & Torbert, R. (1982). On the origin and spatial event of high-latitude F region irregularities. *Journal of Geophysical Research*, *87*(A6), 4469–4475. https://doi.org/10.1029/JA087iA06p04469

Kil, H., Heelis, R. A., Paxton, L. J., & Oh, S.-J. (2009). Formation of a plasma depletion shell in the equatorial ionosphere. *Journal of Geophysical Research*, *114*(A11), A11302. https://doi.org/10.1029/2009JA014369

Kintner, P. M., & Seyler, C. E. (1985). The status of observations and theory of high latitude ionospheric and magnetospheric plasma turbulence. *Space Science Reviews*, *41*(1–2), 91–129. https://doi.org/10.1007/BF00241347

Knudsen, D. J., Burchill, J. K., Buchert, S. C., Eriksson, A. I., Gill, R., Wahlund, J. E., et al. (2017). Thermal ion imagers and Langmuir probes in the Swarm electric field instruments. *Journal of Geophysical Research*, *122*(2), 2655–2673. https://doi.org/10.1002/2016JA022571

Labelle, J., Kelley, M. C., & Seyler, C. E. (1986). An analysis of the role of drift waves in equatorial spread F. *Journal of Geophysical Research*, *91*(A5), 5513–5525. https://doi.org/10.1029/JA091iA05p05513

Martinis, C., Baumgardner, J., Mendillo, M., Su, S.-Y., & Aponte, N. (2009). Brightening of 630.0 nm equatorial spread-F airglow depletions. *Journal of Geophysical Research*, *114*(A6), A06318. https://doi.org/10.1029/2008JA013931

Materassi, M., Forte, B., Coster, A. J., & Skone, S. (Eds.). (2020). *The dynamical ionosphere*. Elsevier.

Moldwin, M. (2008). An introduction to space weather.

Park, J., Min, K. W., Lee, J.-J., Kil, H., Kim, V. P., Kim, H.-J., et al. (2003). Plasma blob events observed by KOMPSAT-1 and DMSP F15 in the low latitude nighttime upper ionosphere. *Geophysical Research Letters*, *30*(21), 2114. https://doi.org/10.1029/2003GL018249

Pécseli, H. (2016). Low frequency waves and turbulence in magnetized laboratory plasmas and in the ionosphere. https://doi.org/10.1088/978-0-7503-1251-6

Peng, C. K., Buldyrev, S. V., Havlin, S., Simons, M., Stanley, H. E., & Goldberger, A. L. (1994). Mosaic organization of DNA nucleotides. *Physical Review E*, *49*(2), 1685–1689. https://doi.org/10.1103/PhysRevE.49.1685

Pezzopane, M., & Pignalberi, A. (2019). The ESA Swarm mission to help ionospheric modeling: A new NeQuick topside formulation for mid-latitude regions. *Scientific Reports*, *9*(1), 12253. https://doi.org/10.1038/s41598-019-48440-6

Pezzopane, M., Pignalberi, A., Coco, I., Consolini, G., De Michelis, P., Giannattasio, F., et al. (2021). Occurrence of GPS loss of lock based on a Swarm half-solar cycle dataset and its relation to the background ionosphere. *Remote Sensing*, *13*(11), 2209. https://doi.org/10.3390/rs13112209

Pignalberi, A. (2021). TITIPy: A Python tool for the calculation and mapping of topside ionosphere turbulence indices. *Computers & Geosciences*, *148*, 104675. https://doi.org/10.1016/j.cageo.2020.104675

Pignalberi, A., Pezzopane, M., & Nava, B. (2022). Optimizing the NeQuick Topside Scale Height Parameters Through COSMIC/FORMOSAT-3 Radio Occultation Data. *IEEE Geoscience and Remote Sensing Letters*, *19*, 1–5. https://doi.org/10.1109/LGRS.2021.3096657

Prikryl, P., Jayachandran, P. T., Mushini, S. C., & Chadwick, R. (2011). Climatology of GPS phase scintillation and HF radar backscatter for the high-latitude ionosphere under solar minimum conditions. *Annales Geophysicae*, *29*(2), 377–392. https://doi.org/10.5194/angeo-29-377-2011

Schmitt, F. G., & Huang, Y. (2016). Stochastic analysis of scaling time series: From turbulence theory to applications.

Spicher, A., Miloch, W. J., & Moen, J. I. (2014). Direct evidence of double-slope power spectra in the high-latitude ionospheric plasma. *Geophysical Research Letters*, *41*(5), 1406–1412. https://doi.org/10.1002/2014GL059214

Taylor, G. I. (1938). The spectrum of turbulence. *Proceedings of the Royal Society of London. Series A - Mathematical and Physical Sciences*, *164*(919), 476–490. https://doi.org/10.1098/rspa.1938.0032

Tsinober, A. (Ed.). (2009). *An informal conceptual introduction to turbulence*. Springer Verlag.

Tsunoda, R. T. (1988). High-latitude F-region irregularities: A review and synthesis. *Reviews of Geophysics*, *26*(4), 719–760. https://doi.org/10.1029/RG026i004p00719

Tsunoda, R. T., Haggstrom, I., Pellinen-Wannberg, A., Steen, A., & Wannberg, G. (1985). Direct evidence of plasma density structuring in the auroral F region ionosphere. *Radio Science*, *20*(4), 762–784. https://doi.org/10.1029/RS020i004p00762

van den IJssel, J., Encarnação, J., Doornbos, E., & Visser, P. (2015). Precise science orbits for the Swarm satellite constellation. *Advances in Space Research*, *56*(6), 1042–1055. https://doi.org/10.1016/j.asr.2015.06.002

Watanabe, S., & Oya, H. (1986). Occurrence characteristics of low latitude ionosphere irregularities observed by impedance probe on board the Hinotori satellite. *Journal of Geomagnetism and Geoelectricity*, *38*(2), 125–149. https://doi.org/10.5636/jgg.38.125

Wiener, N. (Ed.). (1964). *Time series*. M.I.T. Press.

Xiong, C., Stolle, C., & Lühr, H. (2016). The Swarm satellite loss of GPS signal and its relation to ionospheric plasma irregularities. *Space Weather*, *14*(8), 563–577. https://doi.org/10.1002/2016SW001439

Xiong, C., Stolle, C., & Park, J. (2018). Climatology of GPS signal loss observed by Swarm satellites. *Annales Geophysicae*, *36*(2), 679–693. https://doi.org/10.5194/angeo-36-679-2018

Yokoyama, T., Su, S.-Y., & Fukao, S. (2007). Plasma blobs and irregularities concurrently observed by ROCSAT-1 and Equatorial Atmosphere Radar. *Journal of Geophysical Research*, *112*(A5), A05311. https://doi.org/10.1029/2006JA012044